Using bio-based CaCO₃ functionalized sediment to simultaneously remove

algae and COD through adsorption and sedimentation in water source

3 reservoirs

- 4 Yifan Du^{a,b} Jinbo Zhao^{a,b} Qingping Wang^a Jiacheng Feng^a Jinyi Qin^{©,a,b,*}

 Ming Su^{©,b,c,*}
- ^a School of Civil Engineering, Chang'an University, Xi'an 710064, China.
- ⁷ b Key Laboratory of Environmental Aquatic Chemistry, State Key Laboratory of Regional Environ-
- ment and Sustainability, Research Center for Eco-Environmental Sciences, Chinese Academy of
- 9 Sciences, Beijing 100085, China.
- ^c University of Chinese Academy of Sciences, Beijing 100049, China.
- * Corresponding to: Jinyi Qin (jinyi.qin@chd.edu.cn), Ming Su (mingsu@rcees.ac.cn)

2 Abstract

- In-situ turbidity enhancement can suppress algal growth in reservoirs but often exacerbates chemical oxygen demand (COD) accumulation due to incomplete organic removal. This study presents a biologically synthesized bio-CaCO₃-modified sediment, engineered via 15 Bacillus-induced carbonate precipitation, to simultaneously control algae and reduce COD. The material forms 15-30 nm core-shell clusters with enriched -OH/-COOH groups and mesopores 17 (~19.76 nm), confirmed by SEM, XRD, FTIR, and BET (+1.02 m² g⁻¹). Adsorption tests against Microcystis aeruginosa, Chlorella, and Limnothrix showed Langmuir-type monolayer binding (R² > 0.97) and pseudo-second-order kinetics. XDLVO theory and DFT analysis revealed strong EPS-Bio-CaCO₃ interactions (ΔE_{AB} = 31.28 mJ m⁻²; ΔE_{ads} = -1.07 ev). Optimal conditions (7.5 21 wt% CaCO₃, 56% residual Ca²⁺, 85 min) achieved 93.8% Chl-a removal, 88.6% COD reduction, and 87.5% turbidity control ($R^2 = 0.98$), with minimal Ca^{2+} leaching. By integrating chemisorption, interfacial adhesion, and pore confinement, this material provides a stable, eco-friendly strategy for dual pollutant control and *in-situ* sediment remediation.
- **Keywords:** Micro-nano CaCO₃; Sediment modification; Response surface; Extracellular poly-
- meric substances (EPS); XDLVO.

28 I Introduction

Algal blooms in source water reservoirs pose significant environmental and public health challenges by releasing odorous compounds (Su et al., 2015), organic pollutants, and algal toxins 30 (Wnorowski, 1992). These impacts disrupt aquatic ecosystems, degrade water quality, increase 31 treatment costs, and compromise the reliability of drinking water provision (Huisman et al., 32 2018; Jan et al., 2023). Sediment resuspension (SR) has emerged as a viable in-situ strategy for 33 algal bloom control, primarily by attenuating underwater light and promoting particle-induced sedimentation (Fang et al., 2024). When implemented under well-oxygenated conditions, SR 35 can function not merely as a physical suppression measure but also as a biogeochemical process that promotes nutrient retention—stabilizing phosphorus through Fe-P co-precipitation 37 and limiting the mobilization of redox-sensitive metals (Su et al., 2025)—rather than triggering nutrient release. This dual role addresses concerns over internal loading and underscores SR's potential compatibility with drinking-water reservoir management. Nevertheless, turbulence inherent to SR can mobilize organic matter, increasing chemical oxygen demand (COD). Although SR introduces no external reagents and is therefore inherently suited to potable water applications (Ewis et al., 2022; Srinivasan, 2011), its overall performance is strongly governed by sediment geochemistry and structure—highlighting the necessity for targeted sediment optimisation. In reservoir environments, the adsorption efficiency between suspended sediment particles and algae is generally low due to electrostatic repulsion. Modifying clay particles has been explored as a strategy to enhance their adsorption capacity (Barçante et al., 2020; Bergaya and Lagaly, 2013; Farrokhpay and Bradshaw, 2012; Obaje et al., 2013). Key modification techniques include altering the zeta potential (Li et al., 2015), adjusting suspension viscosity, and increasing the number of exchangeable anions and cations, all of which influence the adsorption flocculation-sedimentation process of clay particles. Common cationic modifiers, such as polyaluminum compounds, quaternary ammonium salts (Cao et al., 2006), polyacrylamide (Yu

et al., 2017), and aluminum chloride/aluminum sulfate (Liu et al., 2016) primarily function by modifying surface functional groups (Cao and Yu, 2003). Beyond inorganic clay modifications, organic compounds such as chitosan (Li et al., 2023; Yin et al., 2021) and starch (Cui et al., 2023; Shi et al., 2016) have been investigated for improving adsorption performance. However, their practical application is often hindered by poor stability in aqueous environments, high self-aggregation tendencies, and elevated costs (Pan et al., 2019). Consequently, recent research has focused on developing low-cost, stable, and biodegradable biological modification methods (Sanghi et al., 2006), which offer a more sustainable and environmentally friendly solution for algal control.

Bacillus sp. BF-VB2 modifies kaolin within a pH range of 4.0–10.0, forming a clay-aggregated flocculant capable of treating high-turbidity wastewater (Bisht and Lal, 2019). Compared with chemical flocculants, bio-modified clay-based flocculants have garnered increasing attention due to their biodegradability and high adsorption efficiency. N, N, N-trimethylglycine-grafted cellulose nanocrystals (CNC), in combination with kaolin, form a clay-aggregated flocculant that effectively removes freshwater *Chlorella* vulgaris and marine *Nannochloropsis oculate* (Blockx et al., 2021). Similarly, chitosan, a biopolymer derived from shrimp and crab shells, binds with clay and soil particles to facilitate pollutant sedimentation (Zou et al., 2006). The surface of sediment particles can be modified by algae-derived polysaccharides, which adsorb multivalent metal cations, bind polar organic molecules, and gradually form soil aggregates through coordination complexes and organic-inorganic interactions (Arduino et al., 1989).

Calcium (Ca) in clay plays a crucial role in soil aggregation, adhering to clay and silicate minerals while forming aggregates with carbonates or Ca hydrates that fill pore spaces (Safar and Whalen, 2023). Building on this, bio-CaCO₃ is most effectively deployed as MICP-derived amorphous/micro-nano "seeds" bearing residual EPS, rather than relying on live-cell formation in the field; once introduced into resuspended sediments, these seeds act as persistent nucleation substrates that continue to grow and transform within the sediment matrix under

ambient pore-water chemistry, thereby delivering the practical benefits of biogenic crystallization without maintaining microbial activity. In MICP, microorganisms such as Bacillus or Sporosarcina mediate carbonate formation via urease or carbonic-anhydrase pathways, and EPS serves as a nucleation template that tunes polymorph selection (e.g., calcite, vaterite) and interfacial reactivity (Zhuang et al., 2018). Biogenically synthesized CaCO₃ commonly exhibits hierarchical textures (e.g., dense core-grainy shell, raft-like or needle-like assemblies) (Chekroun et al., 2004; Pérez and García, 2020), widely interpreted as signatures of EPS-regulated nonclassical crystallization with surfaces enriched in -COOH/-OH that promote electrostatic attraction, multidentate Ca-bridging, and steric entrapment with algal cells and organic macromolecules (Kim et al., 2017; Seifan and Berenjian, 2019). Similarly, alkalinityregulated Thauera can enhance carbonate availability, with CO₂ reacting with Ca²⁺ to yield $micro-/nano-CaCO_3, facilitating\ clay\ aggregation\ (Zhao\ et\ al.,\ 2024).\ Thus, the\ main\ advantage$ of bio-CaCO₃ over chemically synthesized CaCO₃ lies in EPS-mediated organic-inorganic coupling that endows seeds with adaptive polymorph evolution and highly functionalized surfaces, while the in-sediment ("seeded") secondary growth clarifies how benefits are realized operationally; nevertheless, the roles of nanoparticle concentration, pore architecture, and specific surface area—particularly under dynamic resuspension—remain underexplored.

In light of these considerations, we propose that sediment modification via micro-nano CaCO₃ represents a feasible strategy to enhance clay aggregation and adsorption capacity, thereby simultaneously inhibiting algal growth and improving COD removal in source water. In this study, micro-nano CaCO₃-modified sediments were synthesized using *Bacillus* bacteria, which are known for their high urease activity and calcium carbonate precipitation ability. The physicochemical properties, algal inhibition efficiency, and COD reduction performance of the modified sediments were systematically investigated. The underlying mechanisms were elucidated through XDLVO theory and complementary modeling approaches. Furthermore, optimal operational parameters—including micro-nano CaCO₃ dosage and residual free Ca²⁺ dosage—were identified to maximize treatment efficacy. This technology not only addresses the organic pol-

lutant surge linked to sediment resuspension in algal control but also advances in situ ecological restoration by providing a chemical-free, material-efficient solution for water body management.

2 Materials and methods

2.1 Sampling information

The sediment was collected from the 0-10 cm water depth sample of the reservoir river channel 112 of the Lianghui Reservoir in Zhejiang Province China (39°54'39.33"N, 116°24'48.18"E) (Table S1). 113 The sediment was sieved through a 100-mesh sieve and refrigerated at 4°C. Major components 114 were SiO_2 (68.72%) and Al_2O_3 (19.56%) (mass ratio 3.5:1), with minor Fe_2O_3 (4.19%) (Table S2). 115 The activated sludge was collected from the aeration tank of the Fourth Wastewater Treatment 116 Plant in Xi'an. Chlorella was isolated from the Shiguan Reservoir in Shanxi Province (China) and 117 cultured in Aquatic Medium No. 6 (AM-6) at 25 °C under an illumination intensity of 2000 lux, with 118 a 12 h:12 h light-dark photoperiod. Microcystis aeruginosa and Limnothrix sp. were obtained 119 from the Freshwater Algae Culture Collection in the Institute of Hydrobiology, Chinese Academy 120 of Science and were cultured using BG11 culture medium. 121

2.2 Preparation of bio-CaCO₃-modified sediment

Eight liters of *Bacillus* culture extract, containing residual extracellular polymeric substances (EPS) and metabolic products, were introduced into a 12 L jacketed reactor as the organic template for seed formation. The pH was maintained at 8–10 by automated titration with 5 mol L⁻¹ NaOH via an injection pump. Aeration was applied for 1.5 h, and dissolved oxygen (DO) was controlled at 2–5 mg L⁻¹. After 24 h, the supernatant was collected and analyzed for CO_3^{2-} and HCO_3^{-} concentrations to determine the Ca^{2+} dosage required for 2%, 5%, 8%, 10%, and 14% (w/w) micro-/nano-scale bio- $CaCO_3$ seeds. The residual free Ca^{2+} concentration was adjusted to

130 0%, 50%, 100%, or 150% of the measured carbonate alkalinity. Calcium chloride solution was
131 then introduced dropwise under continuous stirring to induce nucleation within the EPS ma132 trix. This procedure produced amorphous/micro-nanocrystalline CaCO₃ seeds enriched with
133 structural defects and EPS coatings, which were used directly in subsequent sediment–water
134 experiments to promote secondary mineral growth and contaminant immobilization.

Modified sediment was prepared by mixing 150 mL of a 25 g L⁻¹ clay suspension with bio-CaCO₃-modified *Bacillus* extract at a 3:1 volume ratio (clay:extract) in a 500 mL beaker. The suspension was stirred at 200 rpm for 30 min to promote surface binding and carbonate precipitation. After 12 h of static aging, the mixture was centrifuged at 4000 rpm for 10 min. The resulting pellet was washed twice with deionized water and oven-dried at 50 °C for 24 h. The dried solid was designated as bio-CaCO₃-modified sediment and used in SEM, XRD, BET, and adsorption analyses.

2.3 Adsorption Kinetics and Isotherm Modeling

Adsorption behavior of algae onto bio-CaCO₃-modified sediment was assessed through kinetic and isotherm experiments using three representative species (*Chlorella vulgaris*, *Microcystis aeruginosa*, and *Limnothrix* sp.). In each experiment, 100 mL of algal suspension was mixed with 50 mL of modified sediment and agitated at 120 rpm and 25 °C. For kinetics, fixed initial Chl-a concentrations (*Chlorella* = 1145 μ g L⁻¹, *M. aeruginosa* = 3273 μ g L⁻¹, *Limnothrix* = 980 μ g L⁻¹) were used, and samples were collected at specific time intervals to fit pseudo-first-order and pseudo-second-order models (Eqs. S1–S5).

Equilibrium studies employed algal suspensions with species-specific Chl-a gradients: *Chlorella vulgaris* (23.5–424.9 μ g L⁻¹), *Microcystis aeruginosa* (91.7–1046.5 μ g L⁻¹), and *Limnothrix* sp. (20.0–91.1 μ g L⁻¹). Each 100 mL of algal solution was mixed with 50 mL of bio-CaCO₃-modified sediment (prepared under optimal conditions), and incubated at 25 °C with shaking at 120 rpm for 4 h to ensure adsorption equilibrium. Following centrifugation (1500 g, 20 min), the supernatants were analyzed for residual Chl-a concentration. Adsorption data were fitted

to Langmuir and Freundlich isotherm models (Eqs. S6–S9), with calculated parameters summarized in Table S6. All experiments were conducted in triplicate to ensure reproducibility.

157 2.4 Interfacial Interaction Analysis (XDLVO and DFT)

Zetas potential of the bio-CaCO₃-modified sediment and algal biomass was measured using a Zetasizer Pro Blue (Malvern, UK). Static contact angles were measured on dried compressed pellets using ultrapure water, formamide, and diiodomethane (DAS3, KRÜSS, Germany). Each measurement was performed in quintuplicate. Surface energy components (Lifshitz-van der Waals, electron donor, and electron acceptor) were calculated using the extended Young's equation (ADAM, 1957; White, 1977) (Eqs. S10-S12), and the detailed calculation of the total energy is described in the appendix (Table S7, Table S8).

Density functional theory (DFT) calculations were performed using the periodic plane-wave approach implemented in VASP with the GGA-PBE functional and DFT-D3 dispersion correction, which has been shown to reliably capture both hydrogen bonding and van der Waals interactions at organic-mineral interfaces (Zhao et al., 2018). SiO₂ (001) and calcite (104) surfaces were constructed according to established crystallographic terminations (Kulkarni et al., 2012), with 169 CaCO₃ nanoclusters representing Ca²⁺ bridging domains, a validated strategy for modeling divalent cation-mediated adhesion (Cruz et al., 2012). Representative monosaccharide fragments 171 from algal EPS, such as glucuronic acid, were selected as model compounds due to their prevalence in EPS and their ability to retain the key -COOH and -OH functionalities responsible for 173 interfacial coordination, while offering computational tractability (Zhu et al., 2019). Adsorption 174 energies (ΔE) were calculated from total energy differences, providing molecular-scale insight 175 into EPS-mineral adhesion mechanisms. Computational details and model structures are pro-176 vided in Supporting Information.

2.5 Determination of Chl-a and COD in water samples

After a 15-min reaction, 10 mL supernatants were collected for analysis. Chl-a and COD were measured according to Chinese standard methods HJ 897-2017 and HJ 828-2017, respectively.

All tests were performed in triplicate, and results are reported as mean values. Removal efficiency was calculated as Eq. 1:

Removal efficiency(%) =
$$\frac{100(C_i - C_f)}{C_i}$$
 (1)

where C_i and C_f are the initial and final concentrations (μ g L⁻¹), respectively. This equation was applied to both Chl-a and COD measurements to evaluate algal inhibition and organic matter removal performance.

2.6 Response surface methodology for process optimization

The effects of three operational variables—micro-nano CaCO₃ mass fraction, residual free Ca²⁺ dosage, and contact time—on Chl-a and COD removal were evaluated using response surface methodology (RSM). A Box-Behnken design (BBD) was implemented via Design Expert 8.0 (Stat-Ease Inc., USA) at a 95% confidence level (Table S4). A quadratic polynomial regression model was used to predict removal efficiency. Detailed model equations and coefficient definitions are provided in Supplementary Eq. (S16).

2.7 Microscopic characterization and structural analysis

The morphological characteristics of the sediment were captured by scanning electron microscopy (SEM) (FEI Quanta 600 FEG, USA), and the surface functional groups were reflected by infrared spectroscopy FTIR (Nicolet™ iS™5, Thermo Scientific, USA).

2.8 Materials and data processing

All the chemical reagents needed for the experiment, such as sodium hydroxide, sodium carbonate, calcium chloride, glucose, and urea, were purchased from Sigma-Aldrich (MO, USA) and confirmed as analytical grade. All experimental data were processed and visualized using Origin 201 2021 and ggplot2 in R (v4.0).

202 3 Results and discussion

203 3.1 Removal Efficiency Modulated by Multivariable Conditions

The removal efficiency of Chl-a and COD by Bio-CaCO $_3$ -modified sediment exhibited distinct nonlinear dependencies on CaCO $_3$ dosage, residual Ca $^{2+}$ dosage, and reaction time (Fig. 1A–1B). For Chl-a, maximum removal (>92%) was achieved at CaCO $_3$ dosages >10% and reaction times >60 min, with residual Ca $^{2+}$ showing negligible influence. The response surface revealed a steep gradient along the CaCO $_3$ axis and a plateau at high dosages and prolonged reaction times, indicating that Chl-a removal was predominantly controlled by sorption site availability and surface-mediated flocculation rather than dissolved Ca $^{2+}$.

This behavior aligns with established mechanisms of Ca-based algal aggregation, where electrostatic interactions and bridging with extracellular polymeric substances (EPS) enhance cell destabilization (Gao et al., 2025; Wu et al., 2024). The minimal impact of residual Ca²⁺ suggests that surface-bound CaCO₃, rather than free ions, drives flocculation, likely through charge neutralization and interparticle bridging (Fig. S1A). The observed plateau implies a saturation effect, where additional CaCO₃ or extended contact time no longer improves efficiency—a critical consideration for optimizing operational parameters in practical applications.

The response surface analysis revealed distinct removal patterns for COD compared to Chl-a (Fig. 1B). Optimal COD removal efficiency (~88%) was achieved at intermediate conditions: 6-

220 8% CaCO₃ dosage, 50%-60% residual Ca²⁺, and 60 min reaction time. This system displayed 221 unique sensitivity to ionic strength, following a parabolic response curve where removal efficiency initially improved with increasing Ca²⁺ concentration but declined sharply beyond 80%. 223 This reversal suggests a transition from beneficial complexation at moderate ionic strength to 224 inhibitory effects at higher dosage, potentially due to competitive binding and oversaturation 225 of active sites (Sengco, 2001; Zhang et al., 2009). These findings highlight the dual role of cal-226 cium ions in COD removal - while CaCO₃ provides the structural framework for adsorption, the 227 dissolved Ca²⁺ dosage critically regulates removal efficiency through modulation of molecular 228 interactions.

To further dissect the role of each individual factor, a single-variable statistical analysis was performed (Fig. 1C). For Chl-a, increasing $CaCO_3$ dosage from 2% to 14% resulted in a significant elevation in median removal efficiency from 76.4% to 91.5% (p < 0.01), with a concomitant narrowing of interquartile ranges (Fig. S1B). A similar trend was observed with reaction time, where removal peaked at 60 min and plateaued thereafter. In contrast, variations in residual Ca^{2+} dosage had negligible impact on Chl-a removal, reinforcing the conclusion that algal aggregation is predominantly driven by solid-phase mineral properties.

In contrast, COD removal exhibited more complex behavior, with residual Ca^{2+} emerging as the dominant control factor. The system showed a clear optimum at 50% Ca^{2+} , with median removal efficiency increasing from 63.2% to 81.6% before declining at higher concentrations (p < 0.05). The wider interquartile ranges observed throughout the COD tests, particularly at elevated Ca^{2+} levels, reflect the system's sensitivity to ionic environment fluctuations and suggest multiple competing interaction mechanisms. This fundamental difference in response patterns between Chl-a and COD removal underscores the distinct physicochemical processes governing particulate versus dissolved pollutant sequestration, with important implications for system optimization in complex water treatment scenarios.

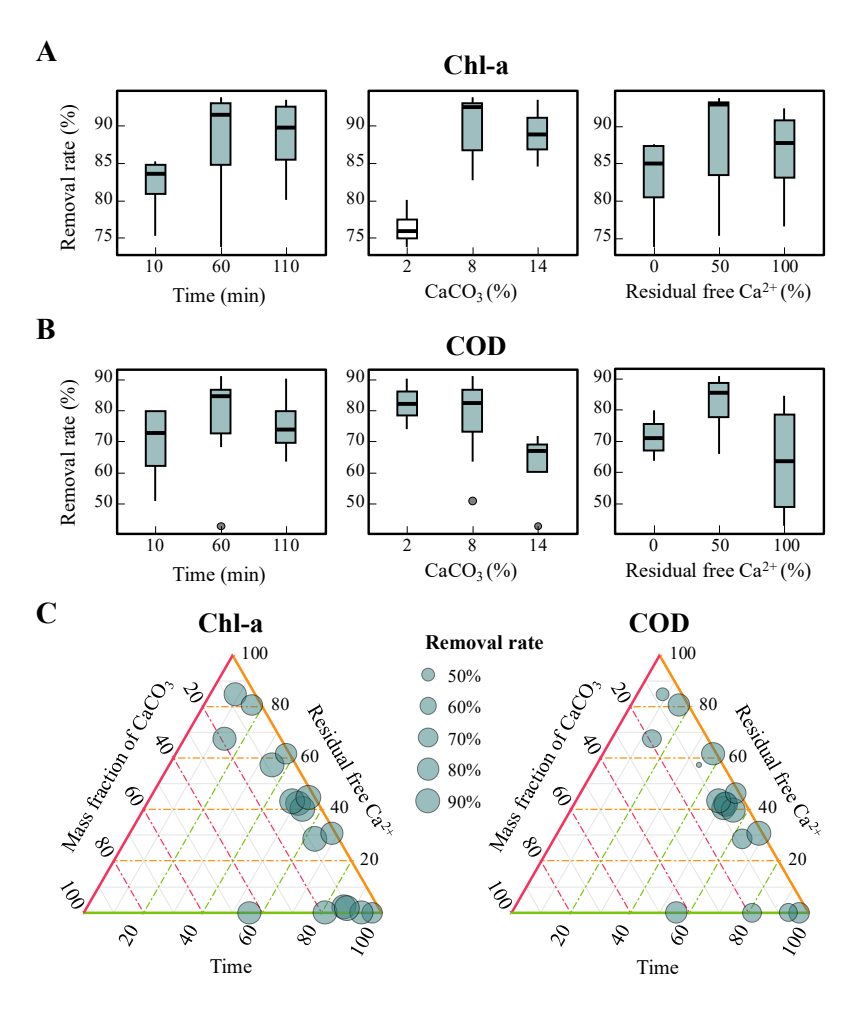


Fig. 1: Bio-CaCO₃-modified sediment removes Chl-a under the combined influence of CaCO₃ mass fraction, residual free Ca²⁺ dosage, and reaction time (A); and removes COD under the same factor combination (B). Chl-a removal rate is influenced by individual parameters including reaction time (10, 60, 110 min), CaCO₃ dosage (2%, 8%, 14%), and residual free Ca²⁺ (0%, 50%, 100%) (C); COD removal rate responds to the same experimental conditions (D).

3.2 Functional-Group Coordination and Interfacial Energetics

Validate Adsorption Kinetics

246

Adsorption of algae onto micro-nano $CaCO_3$ -modified sediment conforms to monolayer chemisorption, as indicated by the higher coefficients of determination (R^2) for both the Langmuir isotherm and the pseudo-second-order (PSO) kinetic model (Fig. S2). The Langmuir model outperformed the Freundlich model (Fig. 2A, Table S6), while the PSO model exhibited R^2 values ranging from 0.971 to 0.997 (Fig. 2B), significantly exceeding those of the pseudo-

first-order (PFO) model (0.533–0.910) (Liu et al., 2020; Zhang et al., 2020). The separation factor $(R_L < 1)$ confirms the thermodynamic feasibility of the process (Table S6). The Langmuir affinity constant (K_L) revealed an order of *Chlorella* (0.011) > *Microcystis aeruginosa* (0.003) \approx *Limnothrix* (0.003), reflecting the relative binding affinities between algal surface functional groups and active sites on the modified sludge (Liu et al., 2020).

At equilibrium, the maximum adsorption capacities $\left(Q_{m}\right)$ of the modified sediment reached 1113 µg g⁻¹ for Microcystis aeruginosa, 617 µg g⁻¹ for Chlorella, and 2699 µg g⁻¹ for Limnothrix, corresponding to differences in initial algal concentration. Experimental equilibrium adsorption capacities (q_e) ranged from 378 to 634 μ g g⁻¹ and were consistent with calculated values (396.8– 260 $662.9~\mu g~g^{-1}$) (Andersen et al., 1991; Safar and Whalen, 2023). Initial adsorption rates followed 261 the order: Microcystis aeruginosa > Limnothrix > Chlorella, which is governed by the initial con-262 centration gradient (Fig. S3). A higher initial concentration (C_0) provides a greater mass transfer 263 driving force, accelerating algal cell diffusion to the adsorbent surface and enhancing the initial 264 adsorption rate (Caliskan et al., 2011). According to the PSO model, the instantaneous adsorp-265 tion rate is proportional to $\frac{dq_t}{dt} \propto k_2 q_e^2$.; at early stages $(q_t \approx 0)$, higher (C_0) values correspond to increased (q_e) , promoting faster initial adsorption (Tran, 2023). 267

The enhanced adsorption performance of *Limnothrix* is attributed to its elevated extracellular 268 polymeric substance (EPS) secretion (Han et al., 2024), which is rich in polysaccharides and an-269 ionic functional groups such as carboxyl and sulfate (Fig. S4). These groups facilitate calcium-270 mediated coordination (e.g., Ca-O bonding), reinforcing interfacial adhesion (Rao et al., 2012). 271 Additionally, the filamentous morphology of *Limnothrix* increases the effective contact area and 272 provides entanglement sites, enhancing spatial compatibility with the porous structure of the 273 modified sludge and contributing to its significantly higher Q_m following modification (Young, 274 2006). 275

Notably, the variation in Chl-a removal efficiency among the three algal species reflects differences in cellular morphology, EPS production, and initial concentration gradients. Fil-

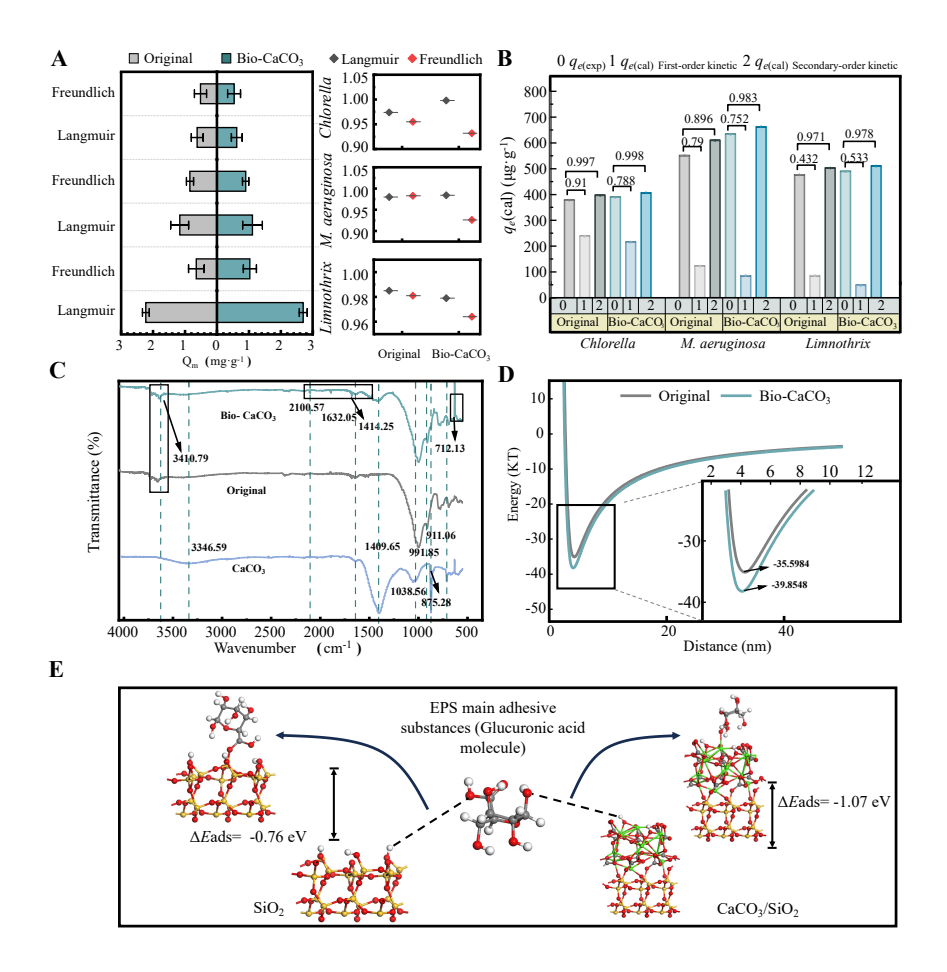


Fig. 2: The adsorption isotherms of Chlorella, Microcystis aeruginosa, and Limnothrix were better described by the Langmuir model than by the Freundlich model, as indicated by higher R² values, suggesting monolayer adsorption onto homogeneous surfaces. The equilibrium adsorption capacities $(q_e, \text{mg g}^{-1})$ were substantially enhanced following Bio-CaCO₃ modification, particularly for Chlorella (A). Adsorption kinetics were more consistent with the pseudo-second-order model, indicating that chemisorption was the rate-limiting mechanism. The modified sediment exhibited markedly improved adsorption rates and capacities across all algal species (B). FTIR absorbance spectra (a.u.) of CaCO₃, original sediment, and Bio-CaCO₃ composites plotted against wavenumber (cm⁻¹) demonstrate enhanced signals corresponding to carbonate groups (v₃: ~1400 cm⁻¹, v₂: ~870 cm⁻¹) and organic functionalities (C=O,-OH), confirming successful biomineral integration (C). Extended DLVO (XDLVO) interaction energy profiles (ΔG_{AB}, mJ m⁻²) plotted against separation distance (nm) reveal that Bio-CaCO₃ surfaces exhibit deeper primary energy minima and lower energy barriers compared to unmodified sediment, indicating stronger attractive interactions (D). Density functional theory (DFT) simulations of glucuronic acid, a representative adhesive saccharide in algal EPS, interacting with sediment surfaces. The adsorption energy (ΔE_{ads}) on pristine SiO₂ is -0.76 eV, whereas the energy decreases to -1.07 eV on CaCO₃-modified SiO₂, indicating stronger interfacial binding after mineral modification (E).

amentous *Limnothrix* sp. exhibited higher removal rates due to its tendency to form dense flocs via self-entanglement and Ca²⁺-mediated EPS bridging, thereby enhancing sedimentation and incorporation into bio-CaCO₃ aggregates (Han et al., 2024). In contrast, *Microcystis* aeruginosa forms buoyant colonies stabilized by gas vesicles, rendering it less susceptible to gravitational settling or bridging flocculation (Verspagen et al., 2006). Additionally, kinetic experiments employed fixed, high initial Chl-a concentrations, whereas equilibrium assays used species-specific gradients (Mackay et al., 2016), further contributing to variability in adsorption behavior. While these differences do not undermine the demonstrated effectiveness of the modified sediment, they underscore the interplay of multiple removal mechanisms—adsorption, bridging, and sedimentation—whose relative contributions vary across algal taxa. Future work will incorporate direct biomass quantification, and EPS characterization to more accurately resolve the dominant removal pathways (Deng et al., 2019; Lai et al., 2018).

284

285

286

287

288

289

Complementary spectroscopic and theoretical analyses collectively elucidate the enhanced 290 algae-sediment interaction mechanisms induced by bio-CaCO₃ modification. FTIR spectra 291 of the modified sediment revealed carbonate vibrational bands at 1414, 875, and 712 cm⁻¹ 292 (aragonite/vaterite phases)(Andersen et al., 1991; Nilsen et al., 2004; Zou et al., 2019), together 293 with hydroxyl peaks at 3612 and 3400 cm⁻¹ (Al-OH, adsorbed -OH) and amide/carboxyl absorp-294 tions at ~1630 cm⁻¹ (Fig. 2C), confirming the retention of EPS-derived organic moieties and 295 indicating organic-inorganic coupling between residual EPS and the mineral phase (Alexander 296 et al., 2018; Andersen et al., 1991; Sand et al., 2011). DFT simulations using glucuronic acid as 297 a model EPS ligand showed that, on silanol-rich silica, carboxyl oxygen atoms formed strong 298 hydrogen bonds (1.62–1.78 Å) with surface Si-OH groups, contracting the C-O-Si bond length 299 from 1.39 Å to 1.33 Å and reducing the O-C-O bond angle from ~166° to ~138°, consistent 300 with reorientation of surface hydroxyls to accommodate the saccharide (Fig. S11A-D). The 301 adsorption energy was ΔE_ads = -0.76 eV, reflecting moderately strong but reversible binding (Yu et al., 2011; Yu et al., 2024). On Ca²⁺-modified surfaces, a dual-binding mode emerged, where Ca²⁺ bridged carboxylate oxygens of glucuronic acid and oxygen atoms from surface silanols (Ca–O: 1.92–2.08 Å) (Fig. S11E-H), increasing stability (ΔE_{ads})=-1.07ev, ~40% stronger) (Fig. 2E) (Desmond et al., 2017). The corresponding dynamic structural evolution can be visualized in the GIF animations for C-Si-O (Fig. S9) and Ca-Si-O (Fig. S10), which clearly

show the persistence of Ca–O coordination and the more rigid adsorption geometry on Ca $^{2+}$ -modified surfaces. Time-resolved trajectories indicated slower relaxation and persistent Ca–O coordination, supporting a multi-point anchoring mechanism that restricts conformational mobility and reduces desorption under shear. At the interfacial scale, XDLVO analysis showed deepening of the primary minimum from $-36.8 \ kT$ to $-40.8 \ kT$ after bio-CaCO $_3$ modification (Fig. 2D) (Wu et al., 2020), indicating stronger attractive forces and greater colloidal stability (Table S8). The consistency between molecular-level DFT results and interface-level XDLVO findings provides strong evidence that Ca $^{2+}$ -mediated hydrogen bonding and cation bridging dominate the enhanced EPS-mineral adhesion, with organic-inorganic coupling, molecular coordination, and interfacial energy optimization acting synergistically.

3.3 Structural refinement of sediment induced by Bio-CaCO₃ integration

The addition of micro-nano CaCO₃ results in substantial changes in the sediment pore structure. 320 The mesopore proportion increases to 73.5%, and the BET-specific surface area rises from 10.08 321 to 11.71 m² g⁻¹ (Fig. 3A), improving structural openness and enlarging the interaction interface 322 with algal cells (Bennett et al., 2012). This structural refinement promotes multi-site adsorption 323 of organic matter within and between clay mineral particles (Kleber et al., 2015). While the mi-324 cropore volume remains stable, the total pore volume expands from 10.55 to 12.44 cm³ g⁻¹, and 325 the average pore diameter decreases from 20.17 nm to 18.39 nm, reflecting a finer and more 326 complex pore network (Fig. 3B). The unmodified sediment exhibited an angular, lamellar morphology with loosely aggregated 328 clay minerals. In contrast, the bio-CaCO₃-modified sediment displayed a uniform coating of 329

spherical particles (15–30 nm), which at higher magnification (200 k×) revealed dense-core and

rough-shell features composed of ~20 nm nodular subunits (D₁ = 19.76 nm) (Fig. 3D-E). These

nanospheres were embedded within the clay matrix, forming grape-like aggregates and a hi-

330

331

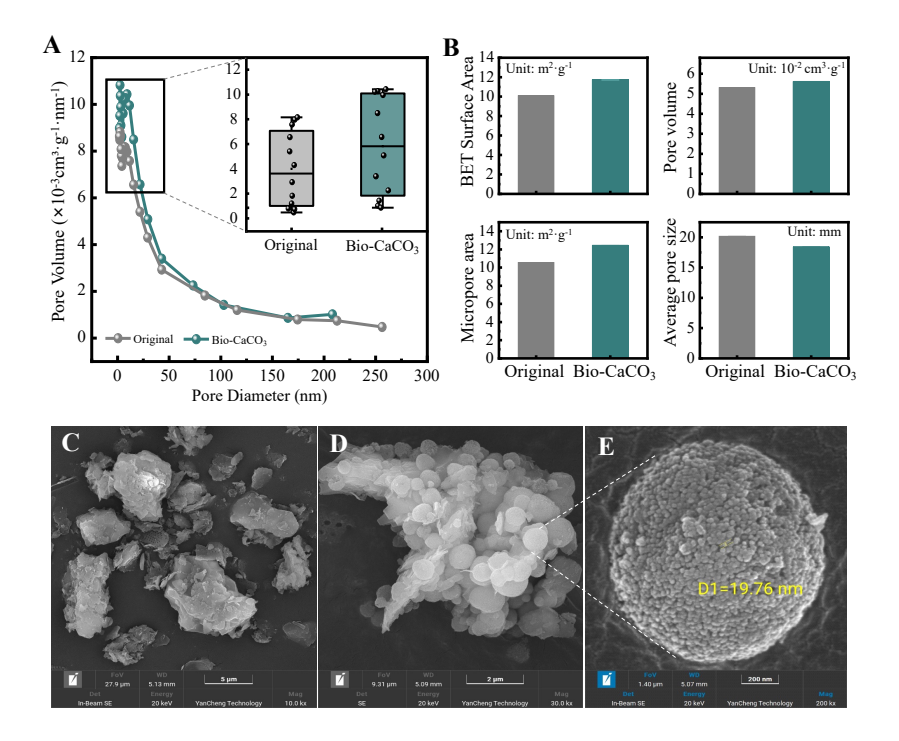


Fig. 3: Particle size distribution curves before and after modification. The modified sample shows a significant shift towards finer particles, as indicated by the red-marked region and arrow. Insets show the statistical distribution of D10, D50, and D90 values (n = 5) (A). Comparison of specific surface area and porosity between original and Bio-CaCO₃-modified samples (B). SEM image of raw sediment particles, showing irregular, compact, and angular morphology (C). SEM image of Bio-CaCO₃-modified particles, forming aggregated spherical structures with increased porosity (D). High-resolution SEM of a single spherical Bio-CaCO₃ particle (D₁ ≈ 19.76 nm), showing a nanoscale porous surface, favorable for enhanced adsorption and surface interaction (E).

erarchical pore framework (Fig. S8). XRD analysis further confirmed that bio-modification induced in-situ CaCO₃~ formation, with pronounced calcite reflections at 2θ ≈ 29.4° (104), 35.9° 334 (110), 39.4° (113), and 47.5° (018) (PDF#05-0586), accompanied by a broad amorphous hump 335 spanning ~20–35° 2θ (Fig. S5). The coexistence of well-defined calcite peaks and an amorphous 336 background is indicative of partial crystallization from an amorphous calcium carbonate (ACC) 337 precursor, a transformation pathway commonly associated with EPS-mediated nonclassical nu-338 cleation (Rodriguez-Navarro et al., 2016; Rodríguez-Navarro et al., 2016). The absence of calcite 339 peaks in the unmodified sediment excludes the possibility of inheritance from the raw mate-340 rial, confirming that crystalline domains were generated during the bio-modification process. 341 Moreover, the relatively low peak intensities and broadened full width at half maximum (FWHM) 342 suggest nanocrystalline dimensions and lattice disorder, consistent with the presence of defectrich seeds capable of continued polymorphic transformation within the sediment microenvironment.

The combination of nanospherical morphology and crystalline phase transformation suggests the successful formation of bio-synthesized micro/nano-scale CaCO₃ on the sediment surface. This hierarchical pore structure facilitates electron transfer and the directional aggregation of amino acids and small proteins (Wang, 2016), regulates the microbial membrane microenvironment, and promotes the self-organization of CaCO₃ into a mesopore-dominated architecture. The morphological evolution aligns with EPS-mediated nucleation and self-assembly mechanisms reported for biogenic minerals, underscoring the synergistic role of microbial interfaces in directing pore-scale organization and improving the capacity for algal and COD removal (Nilsen et al., 2004; Zou et al., 2019).

Notably, the formation of organized CaCO₃ nanostructures is accompanied by the development of moderately hydroxylated surfaces, as revealed by FTIR and supported by DFT analysis (Section 3.2). These surfaces provide reactive Ca–OH sites capable of multidentate complexation with EPS functional groups, reinforcing the interfacial affinity established by the hierarchical morphology. This structural-chemical consistency validates the dual role of bio-CaCO₃ in promoting both surface reactivity and architectural stabilization, thereby supporting the observed enhancements in EPS retention and overall removal performance (Bowers et al., 2015).

3.4 Predictive Modeling of Dual Pollutant Removal Using Box-Behnken Design

362

363

F value or p value is often used to evaluate the significance of each influencing factor in the regression model (Zou et al., 2006). The model equation was evaluated by analysis of variance (ANOVA) (Table S9). Only when the test condition of p < 0.05 was the model and the influencing factor considered significant (Table 1).

Table 1: ANOVA analysis for Chl-a and COD removal regression. (*p values > 0.05 were considered to be not statistically significant.)

Model term	Coefficient	<i>F</i> -value	<i>P</i> -value	Coefficient	<i>F</i> -value	<i>P</i> -value
Response		Chl-a			COD	
prob	< 0.0001			<0.0001		
R^2	0.9939			0.9827		
Pred. R ²	0.9187			0.8054		
CV (%)	0.95			3.64		
Intercept	93.30	126.91	< 0.0001	87.52	44.10	< 0.0001
Α	6.27	466.53	< 0.0001	-10.00	105.76	< 0.0001
В	1.63	31.31	0.0008	-3.87	15.83	0.0053
С	3.15	118.03	< 0.0001	3.17	10.63	0.0139
AB^{\star}	-0.08	0.00946	0.9251	-9.01	42.99	0.0003
AC	1.04	6.35	0.0398	-1.16	0.71	0.4285
BC^*	1.26	2.35	0.1689	10.39	57.10	0.0001
A^2	-7.40	341.29	< 0.0001	-5.45	16.52	0.0048
B^2	-3.86	92.99	< 0.0001	-14.68	120.02	< 0.0001
C ²	-2.55	40.58	0.0004	-5.19	15.01	0.0061

The coefficient of variation (CV%) of the model reflects the relative dispersion of the data. The lower the value, the smaller the dispersion of the data set. In this study, the maximum value of the coefficient of variation (CV%) of COD removal efficiency was 7.31% (far below the 15% threshold), confirming the reliability of the experimental data (Yetilmezsoy et al., 2009).

The response-surface analysis indicates two fundamentally different interaction regimes. For Chl-a, only the AC term ($CaCO_3 \times time$) is significant (F = 6.35, p = 0.040), pointing to a time-dependent generation of chemisorption sites. During the first hour, moderate dosages (4–6 wt

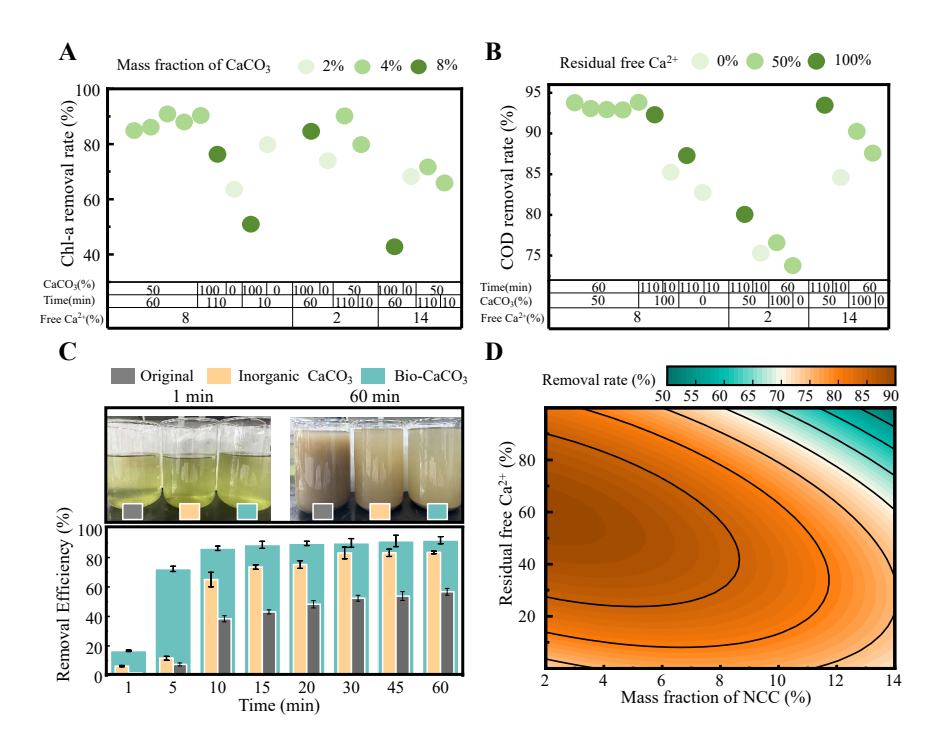


Fig. 4: Bio-CaCO₃-modified sediment achieves optimal Chl-a removal efficiency under the combined effects of CaCO₃ dosage, residual free Ca²⁺ dosage, and reaction time, with CaCO₃ dosage identified as the dominant factor (A). COD removal efficiency under the same conditions is primarily influenced by residual free Ca²⁺ concentration (B). Turbidity reduction during the resuspension–settling process reflects the sediment's flocculation-enhancing effect (C). Interactive effects of CaCO₃ dosage and residual free Ca²⁺ on COD removal efficiency are shown in a response surface plot, indicating a non-linear synergistic relationship (D).

%) (Fig. 4A) recrystallise into calcite/vaterite nanospheres whose freshly exposed Ca–OH groups form inner-sphere complexes with uronic and sulfonic residues in algal EPS ($\Delta E_{\rm ads} \approx -1.07 \, {\rm eV}$) (Li and Stenstrom, 2014; Okoth et al., 2008). When these sites approach saturation (~93 % removal) the uptake curve flattens, and neither higher dosage nor extended contact adds benefit—hence the non-significance of BC (Ca²⁺×time). This behaviour agrees with reports that particulate algal destabilisation is governed by solid-phase Ca sites rather than bulk Ca²⁺ concentration (Keiluweit and Kleber, 2009).

377

378

379

380

38

Notably, the response surface analysis (Fig. 4D) reveals steep gradients and pronounced curvature, indicating a strong nonlinear synergy between $CaCO_3$ dosage and residual Ca^{2+} in enhancing COD removal. Under optimal conditions ($\approx 6-8$ wt% $CaCO_3$, residual $Ca^{2+} \le 60\%$), divalent Ca^{2+} serves as an electrostatic bridge between carboxylate and phenolic groups in dissolved organics and silanol (Si–O) or aluminol (Al–OH) groups on mineral surfaces (Keiluweit and Kleber, 2009; Najafi et al., 2021). Simultaneously, $CaCO_3$ -induced mesoporosity increases the accessible binding surface area, while hydrolysis-derived bicarbonate promotes the accumulation of hydrophilic α -helical proteins in algal EPS, enhancing microalgae–sediment adhesion (Adam-czyk et al., 1992; Safar and Whalen, 2023). Moderate free Ca^{2+} levels (\approx 8–10%) also facilitate coordination with algal carboxyl groups, promoting aggregation and further stabilizing flocs (Cao et al., 2025).

In contrast, when residual Ca²⁺ exceeds ≈ 80%, the system enters an inhibitory regime. Excessive Ca²⁺ compresses the electric double layer, reverses surface charge, and displaces weakly bound fulvate, thereby suppressing COD adsorption (Najafi et al., 2021). This is further supported by 395 the positive coefficient of the Ca²⁺ × time (BC) interaction term in the quadratic model, reflect-396 ing that prolonged contact intensifies Ca²⁺ accumulation and exacerbates adsorption decline— 397 consistent with observations from carbonate-rich riverine systems (Safar and Whalen, 2023). El-398 evated Ca2+ also electrostatically shields Si-O and Al-OH groups, weakening their hydrogen-399 bonding capacity with organics (Greenland and Quirk, 1962; Sand et al., 2011). These results 400 underscore the need for precise regulation of CaCO₃ dosage, Ca²⁺ levels, and reaction time to 40 I sustain the favorable coordination regime while avoiding overloading effects that impair treat-402 ment efficiency. 403

According to the specific parameters (Table 1), the regression model is statistically significant at the 95% confidence level. The regression equations of the predicted response surface quadratic model are shown in Eq. (11) and Eq. (12):

$$Y_1(\%) = 61.206 + 4.132A + 0.173B + 0.145C + 0.00345AC - 0.205A^2 - 0.0015B^2 - 0.001C^2$$
 (11)

$$Y_2(\%) = 67.676 + 2.487A + 0.5B + 0.136C - 0.030AB + 0.0042BC - 0.151A^2 - 0.0058B^2 - 0.0021C^2$$
(12)

The dosage of micro-nano CaCO₃ was 7.5%, the residual free Ca²⁺ was 56%, the contact time was 85.35 min, and the maximum removal rates of Chl-a and COD were 93.83% and 88.64%,

respectively (Table S10).

Biologically modified sediment exhibits markedly enhanced stability during the resuspension process, achieving over 90% reduction in suspended particulate levels within 60 minutes (Fig. 4C). After 30 minutes, the measured value drops to 48.6 NTU, significantly lower than those observed for inorganic-modified (81.3 NTU) and unmodified sediments (231 NTU). This improved performance under both short- and long-term conditions indicates stronger resistance to hydrodynamic disturbance and more effective maintenance of water clarity (Fig. S7). These findings support the use of micro-nano CaCO₃-based biological modification as a low-disturbance and efficient strategy for algal control and aquatic environmental enhancement.

3.5 Synergistic Effects of Surface Potential and Mn Redox Cycling

The surface electrical properties are pivotal for modulating algal removal efficiency (Yu et al., 1995). Bio-CaCO₃ modification led to a Zeta potential shift from -13.2 mV to -9.65 mV, attenuating electrostatic repulsion between negatively charged algal cells and sediment particles. Simultaneously, the extended DLVO interaction energy (ΔG_{AB}) increased from 26.373 to 31.282 mJ m⁻², indicating enhanced exposure of electron-donating groups and stronger interfacial interactions.

The improved performance of the bio-CaCO₃-modified sediment can be attributed to several interconnected mechanisms that operate consistently across molecular, interfacial, and geo-chemical scales. First, the modification process enriches the sediment surface with hydroxy-lated sites and Ca^{2+} -mediated bridging domains (Woods Jr, 2004), increasing the density of active coordination points for algal EPS and mineral particles. Second, extended XDLVO analysis revealed a deeper secondary minimum (-40.8 kT compared to -36.8 kT for unmodified sediment), which favors reversible adsorption and temporary retention, while the high primary barrier (~1900 kT)) inhibits irreversible fouling (Adamczyk et al., 1992). Third, the enhanced EPS-

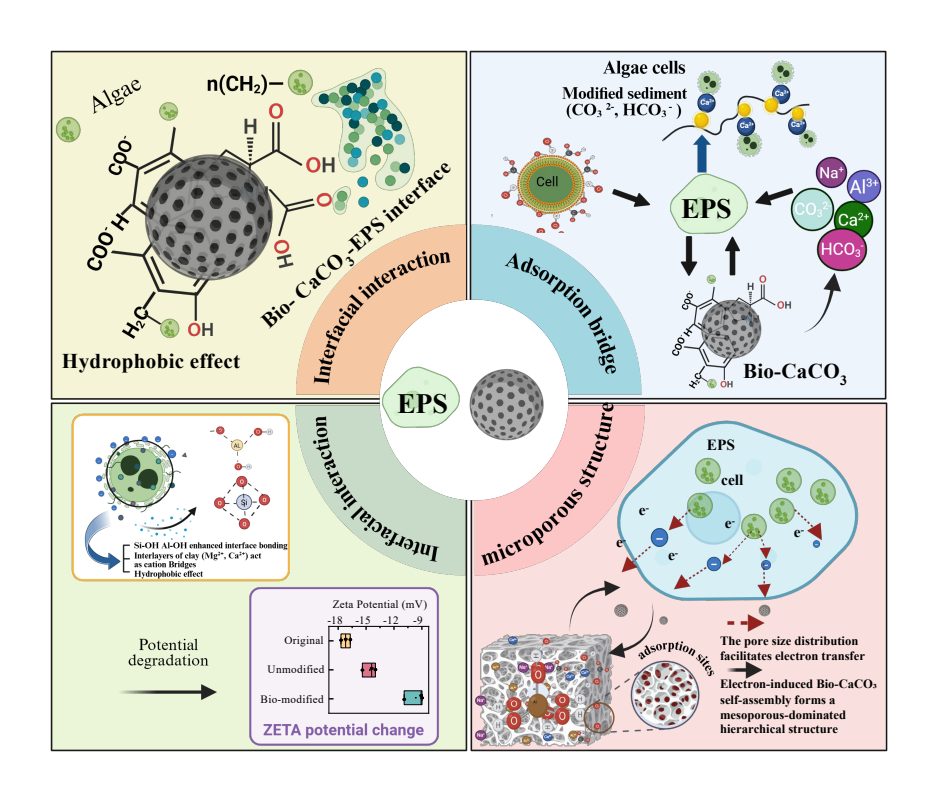


Fig. 5: Schematic illustration of the interaction mechanisms between Bio-CaCO₃-modified sediment and algal extracellular polymeric substances (EPS).

surface interaction—particularly with the bound EPS fraction—was associated with a 15.3% reduction in contact angle, indicating increased surface hydrophobicity that further promotes controlled cell attachment. Together, these effects yield an interface that combines strong yet reversible binding, preventing both inefficient capture and long-term blockage.

Additionally, manganese (Mn) fractionation was employed as a redox-sensitive geochemical tracer to evaluate the interfacial behavior of the bio-CaCO₃-modified sediment (Su et al.,

2025). Under aerobic sediment resuspension, where dissolved oxygen exceeded 5 mg L⁻¹, the dispersion of bio-CaCO₃ seeds within the sediment matrix provided persistent nucleation sites for continuous *in-situ* crystal growth, while maintaining an oxidative microenvironment that is known to suppress internal nutrient release through Fe–P co-precipitation. This environment also likely promoted the activity of indigenous Mn-oxidizing bacteria, facilitating the oxidation of soluble Mn²⁺ to higher-valent particulate Mn species (e.g., Mn³⁺/Mn⁴⁺ oxides) (Tebo et al., 2005; Zhou and Fu, 2020). These oxidized Mn forms, though not the primary removal pathway,

can form coordination complexes or co-precipitate with CaCO₃ and algal EPS, contributing to aggregate formation and interfacial stabilization (Pulsawat et al., 2003). Correspondingly, a no-45 I table shift from exchangeable and reducible Mn to more stable oxidized fractions was observed, indicating enhanced mineral-organic complexation and reduced ion mobility. Given that Mn 453 speciation responds sensitively to redox and binding environment changes, this behavior 454 serves as an indirect indicator of adsorption strength and interface robustness. These coupled 455 processes—surface potential modification by Ca²⁺-mediated organic-inorganic coupling and 456 Mn redox cycling under well-oxygenated SR—collectively support the dual removal of Chl-a 457 and COD via adsorption-driven pathways without stimulating nutrient release. 458

459 4 Conclusion

Bio-CaCO₃ functionalisation of reservoir sediment enables efficient, in-situ control of algal biomass and dissolved organics during resuspension, achieving up to 92% Chl-a and 88% COD removal at the optimal condition (7.5 wt% CaCO₃, 56% residual Ca²⁺, 85 min). The bio-mineral coating forms 15–30 nm CaCO $_3$ nanospheres, increasing BET surface area (10.1 \rightarrow 463 11.7 $\mathrm{m^2~g^{\text{-1}}}$) and generating ~18 nm mesopores, serving as crystallisation seeds that drive and 464 sustain amorphous-to-crystalline transformation within the sediment matrix. This process 465 preserves organic-inorganic coupling with residual EPS, while Ca²⁺ release modulates surface 466 potential (-13.2 → -9.7 mV) and deepens the secondary XDLVO minimum, enhancing reversible 467 EPS-mediated adhesion. Together with the redox-responsive sediment microenvironment, 468 these structural and chemical attributes create a self-regenerating interface capable of main-469 taining high removal performance under dynamic reservoir conditions, offering a practical and 470 environmentally benign strategy for long-term water quality protection. 471

5 Acknowledgements

This work was supported by the National Natural Science Foundation of China (Grant No 52030002), the Key R&D Program of Shaanxi Province (Grant No. No 2024SF-YBXM-535), the National Natural Science Foundation of China (Grant No. No 51808044), and the Qinchuangyuan "Scientist + Engineer" Team Construction Project of Shaanxi Province (Grant No. No 2022KXJ-119). We also extend our sincere gratitude to Dr. Guangyu An for his invaluable assistance with the DFT analysis in this study.

References

- ADAM, N.K., 1957. Use of the term "young's equation" for contact angles. Nature 180, 809–810.

 https://doi.org/10.1038/180809a0
- Adamczyk, Z., Siwek, B., Zembala, M., 1992. Reversible and irreversible adsorption of particles on homogeneous surfaces. Colloids and Surfaces 62, 119–130. https://doi.org/10.1016/0166-6622(92)80043-2
- Alexander, J.A., Ahmad Zaini, M.A., Surajudeen, A., Aliyu, E.-N.U., Omeiza, A.U., 2018. Surface modification of low-cost bentonite adsorbents—a review. Particulate Science and Technology 37, 538–549. https://doi.org/10.1080/02726351.2018.1438548
- Andersen, F.A., Brecevic, L., Beuter, G., Dell'Amico, D.B., Calderazzo, F., Bjerrum, N.J., Underhill,
 A.E., 1991. Infrared spectra of amorphous and crystalline calcium carbonate. Acta Chem.
 Scand 45, 1018–1024.
- Arduino, E., Barberis, E., Boero, V., 1989. Iron oxides and particle aggregation in b horizons of some italian soils. Geoderma 45, 319–329. https://doi.org/10.1016/0016-7061(89)90014-1

 Barçante, B., Nascimento, N.O., Silva, T.F.G., Reis, L.A., Giani, A., 2020. Cyanobacteria dynam-
- ics and phytoplankton species richness as a measure of waterbody recovery: Response to phosphorus removal treatment in a tropical eutrophic reservoir. Ecological Indicators 117,

```
Bennett, R.H., Hulbert, M.H., Curry, K.J., Curry, A., Douglas, J., 2012. Organic matter sequestered
        in potential energy fields predicted by 3-d clay microstructure model. Marine Geology 315-
498
        318, 108–114. https://doi.org/10.1016/j.margeo.2012.04.009
499
    Bergaya, F., Lagaly, G., 2013. General introduction, in: Handbook of Clay Science. Elsevier, pp.
500
        1-19. https://doi.org/10.1016/b978-0-08-098258-8.00001-8
501
    Bisht, V., Lal, B., 2019. Exploration of performance kinetics and mechanism of action of a poten-
502
       tial novel bioflocculant BF-VB2 on clay and dye wastewater flocculation. Frontiers in Micro-
503
        biology 10. https://doi.org/10.3389/fmicb.2019.01288
504
    Blockx, J., Verfaillie, A., Deschaume, O., Bartic, C., Muylaert, K., Thielemans, W., 2021. Glycine
505
        betaine grafted nanocellulose as an effective and bio-based cationic nanocellulose floccu-
506
        lant for wastewater treatment and microalgal harvesting. Nanoscale Advances 3, 4133–4144.
507
        https://doi.org/10.1039/d1na00102g
508
    Bowers, G.M., Argersinger, H.E., Reddy, U.V., Johnson, T.A., Arey, B., Bowden, M., Kirkpatrick,
509
        R.J., 2015. Integrated molecular and microscopic scale insight into morphology and ion dy-
510
        namics in Ca2+-mediated natural organic matter floccs. The Journal of Physical Chemistry
511
       C 119, 17773–17783. https://doi.org/10.1021/acs.jpcc.5b05509
512
    Caliskan, N., Kul, A.R., Alkan, S., Sogut, E.G., Alacabey, İ., 2011. Adsorption of zinc(II) on di-
513
        atomite and manganese-oxide-modified diatomite: A kinetic and equilibrium study. Jour-
514
        nal of Hazardous Materials 193, 27–36. https://doi.org/10.1016/j.jhazmat.2011.06.058
515
    Cao, D.-Q., Song, Y.-X., Wu, Y.-F., Yihuo, G., Jin, J.-Y., 2025. Calcium ion mixing modes govern
        membrane fouling mitigation during membrane-based recovery of extracellular polymeric
517
        substances. Membranes 15, 169. https://doi.org/10.3390/membranes15060169
    Cao, X., Song, X., Yu, Z., Wang, K., 2006. [Mechanisms of removing red tide organisms by organo-
519
        clays]. Huan Jing Ke Xue 27, 1522–1530.
520
    Cao, X., Yu, Z., 2003. [Extinguishment of harmful algae by organo-clay]. Ying Yong Sheng Tai Xue
521
        Bao = The Journal of Applied Ecology 14, 1169–1172.
522
```

106702. https://doi.org/10.1016/j.ecolind.2020.106702

496

- 523 Chekroun, K.B., Rodriguez-Navarro, C., Gonzalez-Munoz, M.T., Arias, J.M., Cultrone, G.,
- Rodriguez-Gallego, M., 2004. Precipitation and growth morphology of calcium carbonate
- induced by myxococcus xanthus: Implications for recognition of bacterial carbonates.
- Journal of Sedimentary Research 74, 868–876. https://doi.org/10.1306/050504740868
- 527 Cruz, L.F., Cobine, P.A., De La Fuente, L., 2012. Calcium increases xylella fastidiosa surface at-
- tachment, biofilm formation, and twitching motility. Applied and Environmental Microbiol-
- ogy 78, 1321–1331. https://doi.org/10.1128/aem.06501-11
- ⁵³⁰ Cui, J., Niu, X., Zhang, D., Ma, J., Zhu, X., Zheng, X., Lin, Z., Fu, M., 2023. The novel chitosan-
- amphoteric starch dual flocculants for enhanced removal of microcystis aeruginosa and al-
- gal organic matter. Carbohydrate Polymers 304, 120474. https://doi.org/10.1016/j.carbpol.
- 533 2022.120474
- Deng, X., Qi, M., Ren, R., Liu, J., Sun, X., Xie, P., Chen, J., 2019. The relationships between odors
- and environmental factors at bloom and non-bloom area in lake taihu, china. Chemosphere
- 218, 569–576. https://doi.org/10.1016/j.chemosphere.2018.11.121
- Desmond, J.L., Juhl, K., Hassenkam, T., Stipp, S.L.S., Walsh, T.R., Rodger, P.M., 2017. Organic-
- silica interactions in saline: Elucidating the structural influence of calcium in low-salinity
- enhanced oil recovery. Scientific Reports 7. https://doi.org/10.1038/s41598-017-10327-9
- Ewis, D., Ba-Abbad, M.M., Benamor, A., El-Naas, M.H., 2022. Adsorption of organic water pollu-
- tants by clays and clay minerals composites: A comprehensive review. Applied Clay Science
- 229, 106686. https://doi.org/10.1016/j.clay.2022.106686
- Fang, J., Li, Y., Su, M., Cao, T., Sun, X., Ai, Y., Qin, J., Yu, J., Yang, M., 2024. Mitigating harmful
- cyanobacterial blooms in drinking water reservoirs through in-situ sediment resuspension.
- Water Research 267, 122509. https://doi.org/10.1016/j.watres.2024.122509
- Farrokhpay, S., Bradshaw, D., 2012. Effect of clay minerals on froth stability in mineral flotation.
- A review, XXVI. IMPC, New Delhi, India, Paper 313.
- 548 Gao, X., Zhang, H., Zhang, X., Zhang, C., Mao, C., Shan, S., Wei, F., Mortimer, M., Fang, J., 2025.
- Interactions between extracellular polymeric substances and engineered nanoparticles in

```
aquatic systems and their environmental effects: A comprehensive review. Environmental
550
       Science: Nano 12, 2177–2192. https://doi.org/10.1039/d5en00073d
    Greenland, D.J., Quirk, J.P., 1962. Adsorption of 1-n-alkyl pyridinium bromides by montmoril-
       lonite, in: Clays and Clay Minerals. Elsevier, pp. 484–499. https://doi.org/10.1016/b978-1-
553
       4831-9842-2.50039-0
554
    Han, S.-F., Jin, W., Qu, F., Hanelt, D., Abomohra, A., 2024. Integrated municipal wastewater treat-
555
       ment and lipid accumulation by a self-flocculating/floating microalga limnothrix sp. Biore-
556
       source Technology 394, 130165. https://doi.org/10.1016/j.biortech.2023.130165
557
    Huisman, J., Codd, G.A., Paerl, H.W., Ibelings, B.W., Verspagen, J.M.H., Visser, P.M.,
558
                                          Nature Reviews Microbiology 16, 471–483.
       2018.
                Cyanobacterial blooms.
                                                                                             https:
559
       //doi.org/10.1038/s41579-018-0040-1
560
    Jan, S., Mishra, A.K., Bhat, M.A., Bhat, M.A., Jan, A.T., 2023. Pollutants in aquatic system: A fron-
561
       tier perspective of emerging threat and strategies to solve the crisis for safe drinking water.
562
       Environmental Science and Pollution Research 30, 113242–113279. https://doi.org/10.1007/
563
       s11356-023-30302-4
564
    Keiluweit, M., Kleber, M., 2009. Molecular-level interactions in soils and sediments: The role of
565
       aromatic π-systems. Environmental Science & Technology 43, 3421–3429. https://doi.org/
566
       10.1021/es8033044
567
    Kim, H., Jo, B.Y., Kim, H.S., 2017. Effect of different concentrations and ratios of ammonium, ni-
       trate, and phosphate on growth of the blue-green alga (cyanobacterium) microcystis aerug-
569
       inosa isolated from the nakdong river, korea. ALGAE 32, 275–284. https://doi.org/10.4490/
       algae.2017.32.10.23
571
    Kleber, M., Eusterhues, K., Keiluweit, M., Mikutta, C., Mikutta, R., Nico, P.S., 2015. Mineral-
       organic associations: Formation, properties, and relevance in soil environments, in:
573
       Advances in Agronomy. Elsevier, pp. 1–140. https://doi.org/10.1016/bs.agron.2014.10.005
574
    Kulkarni, A.D., Truhlar, D.G., Goverapet Srinivasan, S., Duin, A.C.T. van, Norman, P., Schwartzen-
575
       truber, T.E., 2012. Oxygen interactions with silica surfaces: Coupled cluster and density func-
576
```

- tional investigation and the development of a new ReaxFF potential. The Journal of Physical
- ⁵⁷⁸ Chemistry C 117, 258–269. https://doi.org/10.1021/jp3086649
- Lai, H., Fang, H., Huang, L., He, G., Reible, D., 2018. A review on sediment bioflocculation: Dy-
- namics, influencing factors and modeling. Science of The Total Environment 642, 1184–1200.
- https://doi.org/10.1016/j.scitotenv.2018.06.101
- Li, B., Stenstrom, M.K., 2014. Research advances and challenges in one-dimensional modeling
- of secondary settling tanks a critical review. Water Research 65, 40–63. https://doi.org/10.
- ⁵⁸⁴ 1016/j.watres.2014.07.007
- Li, H., Yu, Z., Cao, X., Song, X., 2023. Chitosan modification and its synergism with clay to mitigate
- harmful algal blooms. Environmental Technology & Innovation 29, 103028. https://doi.org/
- 587 10.1016/j.eti.2023.103028
- Li, L., Zhang, H., Pan, G., 2015. Influence of zeta potential on the flocculation of cyanobacteria
- cells using chitosan modified soil. Journal of Environmental Sciences 28, 47–53. https://doi.
- org/10.1016/j.jes.2014.04.017
- Liu, L., Liu, X., Wang, D., Lin, H., Huang, L., 2020. Removal and reduction of cr(\(\mathbb{N} \)) in
- simulated wastewater using magnetic biochar prepared by co-pyrolysis of nano-
- zero-valent iron and sewage sludge. Journal of Cleaner Production 257, 120562.
- 594 https://doi.org/10.1016/j.jclepro.2020.120562
- Liu, Y., Cao, X., Yu, Z., Song, X., Qiu, L., 2016. Controlling harmful algae blooms using aluminum-
- modified clay. Marine Pollution Bulletin 103, 211–219. https://doi.org/10.1016/j.marpolbul.
- 597 2015.12.017
- Mackay, D., Celsie, A.K.D., Arnot, J.A., Powell, D.E., 2016. Processes influencing chem-
- ical biomagnification and trophic magnification factors in aquatic ecosystems: Im-
- plications for chemical hazard and risk assessment. Chemosphere 154, 99–108.
- https://doi.org/10.1016/j.chemosphere.2016.03.048
- Najafi, H., Farajfaed, S., Zolgharnian, S., Mosavi Mirak, S.H., Asasian-Kolur, N., Sharifian, S., 2021.
- A comprehensive study on modified-pillared clays as an adsorbent in wastewater treatment

```
processes. Process Safety and Environmental Protection 147, 8–36. https://doi.org/10.1016/
604
       j.psep.2020.09.028
    Nilsen, O., Fjellvåg, H., Kjekshus, A., 2004. Growth of calcium carbonate by the atomic layer
       chemical vapour deposition technique. Thin Solid Films 450, 240-247. https://doi.org/10.
607
       1016/j.tsf.2003.10.152
608
    Obaje, S., Omada, J., Dambatta, U., 2013. Clays and their industrial applications: Synoptic re-
609
       view. International Journal of Science and Technology 3, 264–270.
610
    Okoth, G., Centikaya, S., Brüggemann, J., Thöming, J., 2008. On hydrodynamic optimisation of
611
       multi-channel counter-flow lamella settlers and separation efficiency of cohesive particles.
612
       Chemical Engineering and Processing: Process Intensification 47, 90–100. https://doi.org/
613
       10.1016/j.cep.2007.08.003
614
    Pan, S.-Y., Haddad, A.Z., Gadgil, A.J., 2019. Toward greener and more sustainable manufacture
615
       of bauxite-derived adsorbents for water defluoridation. ACS Sustainable Chemistry & Engi-
616
       neering 7, 18323–18331. https://doi.org/10.1021/acssuschemeng.9b03649
617
    Pérez, H.F., García, M.G., 2020. Bioprecipitation of calcium carbonate by bacillus subtilis and its
618
       potential to self-healing in cement-based materials. Journal of Applied Research and Tech-
619
       nology 18. https://doi.org/10.22201/icat.24486736e.2020.18.5.1280
620
    Pulsawat, W., Leksawasdi, N., Rogers, P.L., Foster, L.J.R., 2003. Anions effects on biosorption of
621
       mn(II) by extracellular polymeric substance (EPS) from rhizobium etli. Biotechnology Letters
622
```

- Rao, K., Kundu, T., Parker, S., 2012. Molecular modeling of mineral surface reactions in flotation.
- Molecular modeling for the design of novel performance chemicals and materials 65–105.

25, 1267–1270. https://doi.org/10.1023/a:1025083116343

623

- Rodriguez-Navarro, C., Burgos Cara, A., Elert, K., Putnis, C.V., Ruiz-Agudo, E., 2016. Direct nanoscale imaging reveals the growth of calcite crystals via amorphous nanoparticles.
- Crystal Growth & Design 16, 1850–1860. https://doi.org/10.1021/acs.cgd.5b01180
- Rodríguez-Navarro, C., Ruiz-Agudo, E., Harris, J., Wolf, S.E., 2016. Nonclassical crystallization in vivo et in vitro (II): Nanogranular features in biomimetic minerals disclose a general colloid-

```
mediated crystal growth mechanism. Journal of Structural Biology 196, 260–287. https://
63 I
       doi.org/10.1016/j.jsb.2016.09.005
632
    Safar, F., Whalen, J.K., 2023. Mechanical stability of newly-formed soil macroaggregates influ-
633
       enced by calcium concentration and the calcium counter-anion. Geoderma 430, 116333.
634
       https://doi.org/10.1016/j.geoderma.2023.116333
635
   Sand, K.K., Rodriguez-Blanco, J.D., Makovicky, E., Benning, L.G., Stipp, S.L.S., 2011. Crystal-
636
       lization of CaCO3in water-alcohol mixtures: Spherulitic growth, polymorph stabilization,
637
       and morphology change. Crystal Growth & Design 12, 842–853. https://doi.org/10.1021/
638
       cg2012342
639
    Sanghi, R., Bhattacharya, B., Dixit, A., Singh, V., 2006. Ipomoea dasysperma seed gum: An effec-
640
       tive natural coagulant for the decolorization of textile dye solutions. Journal of Environmen-
641
       tal Management 81, 36–41. https://doi.org/10.1016/j.jenvman.2005.09.015
642
   Seifan, M., Berenjian, A., 2019. Microbially induced calcium carbonate precipitation: A
643
       widespread phenomenon in the biological world. Applied Microbiology and Biotechnology
644
       103, 4693–4708. https://doi.org/10.1007/s00253-019-09861-5
645
   Sengco, M.R., 2001. The aggregation of clay minerals and marine microalgal cells: Physicochem-
646
       ical theory and implications for controlling harmful algal blooms (Thesis).
647
    Shi, W., Tan, W., Wang, L., Pan, G., 2016. Removal of microcystis aeruginosa using cationic starch
       modified soils. Water Research 97, 19–25. https://doi.org/10.1016/j.watres.2015.06.029
649
    Srinivasan, R., 2011. Advances in application of natural clay and its composites in removal of
       biological, organic, and inorganic contaminants from drinking water. Advances in Materials
651
       Science and Engineering 2011, 1–17. https://doi.org/10.1155/2011/872531
652
    Su, M., Li, W., Fang, J., Cao, T., Ai, Y., Lü, C., Zhao, J., Yang, Z., Yang, M., 2025. Effects of oxy-
653
       genation resuspension on DOM composition and its role in reducing dissolved manganese
654
       in drinking water reservoirs. Environmental Science & Technology 59, 10498–10509. https:
655
       //doi.org/10.1021/acs.est.5c00235
656
```

Su, M., Yu, J., Zhang, J., Chen, H., An, W., Vogt, R.D., Andersen, T., Jia, D., Wang, J., Yang, M.,

- 2015. MIB-producing cyanobacteria (*Planktothrix* sp.) in a drinking water reservoir: Distri-
- bution and odor producing potential. Water Research 68, 444–453. https://doi.org/10.1016/
- i.watres.2014.09.038
- Tebo, B.M., Johnson, H.A., McCarthy, J.K., Templeton, A.S., 2005. Geomicrobiology of man-
- ganese(II) oxidation. Trends in Microbiology 13, 421–428. https://doi.org/10.1016/j.tim.
- 663 2005.07.009
- Tran, H.N., 2023. Applying linear forms of pseudo-second-order kinetic model for feasibly iden-
- tifying errors in the initial periods of time-dependent adsorption datasets. Water 15, 1231.
- https://doi.org/10.3390/w15061231
- Verspagen, J., Visser, P., Huisman, J., 2006. Aggregation with clay causes sedimentation of the
- buoyant cyanobacteria microcystis spp. Aquatic Microbial Ecology 44, 165–174. https://doi.
- org/10.3354/ame044165
- Wang, Z., 2016. The role of biomolecules in hydroxyapatite biomineralization (PhD thesis). Uni-
- versity of Akron.
- White, L.R., 1977. On deviations from young's equation. Journal of the Chemical Society, Fara-
- day Transactions 1: Physical Chemistry in Condensed Phases 73, 390. https://doi.org/10.
- 1039/f19777300390
- Wnorowski, A., 1992. Tastes and odours in the aquatic environment: A review. Water Sa 18,
- 203-214.
- Woods Jr, C.E., 2004. Examination of the effects of biosurfactant concentration on natural gas
- hydrate formation in seafloor porous media. Mississippi State University.
- Wu, K., Ouyang, S., Tao, Z., Hu, X., Zhou, Q., 2024. Algal extracellular polymeric substance com-
- positions drive the binding characteristics, affinity, and phytotoxicity of graphene oxide in
- water. Water Research 260, 121908. https://doi.org/10.1016/j.watres.2024.121908
- 682 Wu, T., Huang, Q., Liu, Z., Wang, Y., Lin, D., 2020. Distribution-balanced loss for multi-label clas-
- sification in long-tailed datasets, in: Computer Vision ECCV 2020. Springer International
- Publishing, pp. 162–178. https://doi.org/10.1007/978-3-030-58548-8_10

- Yetilmezsoy, K., Demirel, S., Vanderbei, R.J., 2009. Response surface modeling of pb(II) removal
- from aqueous solution by pistacia vera l.: Box-behnken experimental design. Journal of
- 687 Hazardous Materials 171, 551–562. https://doi.org/10.1016/j.jhazmat.2009.06.035
- Yin, Z., Chu, R., Zhu, L., Li, S., Mo, F., Hu, D., Liu, C., 2021. Application of chitosan-based floccu-
- lants to harvest microalgal biomass for biofuel production: A review. Renewable and Sus-
- tainable Energy Reviews 145, 111159. https://doi.org/10.1016/j.rser.2021.111159
- Young, K.D., 2006. The selective value of bacterial shape. Microbiology and Molecular Biology
- Reviews 70, 660–703. https://doi.org/10.1128/mmbr.00001-06
- Yu, F.-C., Phalak, N., Sun, Z., Fan, L.-S., 2011. Activation strategies for calcium-based sorbents
- for CO2 capture: A perspective. Industrial & Engineering Chemistry Research 51, 2133–2142.
- 695 https://doi.org/10.1021/ie200802y
- 496 Yu, J., Wang, K., Yang, P., Li, M., Dong, B., Jin, Z., Hong, S., Ma, H., 2024. Simulation of cal-
- cium carbonate nucleation processes in confined c-s-h nanopores with different calcium-
- silicon ratios. Construction and Building Materials 438, 137157. https://doi.org/10.1016/j.
- 699 conbuildmat.2024.137157
- Yu, Z., Song, X., Cao, X., Liu, Y., 2017. Mitigation of harmful algal blooms using modified clays:
- Theory, mechanisms, and applications. Harmful Algae 69, 48–64. https://doi.org/10.1016/j.
- 702 hal.2017.09.004
- Yu, Z., Zou, J., Ma, X., 1995. Application of clays to removal of red tide organisms III. The coag-
- ulation of kaolin on red tide organisms. Chinese Journal of Oceanology and Limnology 13,
- 705 62-70. https://doi.org/10.1007/bf02845350
- ⁷⁰⁶ Zhang, Y., Chen, Y., Westerhoff, P., Crittenden, J., 2009. Impact of natural organic matter and
- divalent cations on the stability of aqueous nanoparticles. Water Research 43, 4249–4257.
- 708 https://doi.org/10.1016/j.watres.2009.06.005
- ⁷⁰⁹ Zhang, Y., Wang, Y., Cao, X., Xue, J., Zhang, Q., Tian, J., Li, X., Qiu, X., Pan, B., Gu, A.Z., Zheng,
- X., 2020. Effect of carboxyl and hydroxyl groups on adsorptive polysaccharide fouling: A
- comparative study based on PVDF and graphene oxide (GO) modified PVDF surfaces. Journal

- of Membrane Science 595, 117514. https://doi.org/10.1016/j.memsci.2019.117514
- Zhao, H., Yang, Y., Shu, X., Wang, Y., Ran, Q., 2018. Adsorption of organic molecules on mineral
- surfaces studied by first-principle calculations: A review. Advances in Colloid and Interface
- Science 256, 230–241. https://doi.org/10.1016/j.cis.2018.04.003
- Zhao, J., Feng, J., Du, Y., Yan, Z., Li, X., Qin, J., Su, M., Yang, M., 2024. Alkalinity control in sludge
- propels the conversion of concrete slurry waste into micro- and nano-sized biogenic CaCO3.
- Water Science & Technology 90, 1070–1081. https://doi.org/10.2166/wst.2024.255
- 719 Zhou, H., Fu, C., 2020. Manganese-oxidizing microbes and biogenic manganese oxides: Char-
- acterization, mn(II) oxidation mechanism and environmental relevance. Reviews in Envi-
- ronmental Science and Bio/Technology 19, 489–507. https://doi.org/10.1007/s11157-020-
- 722 09541-1
- 723 Zhu, W., Chen, T., He, R., Ding, Y., Duan, T., Xiao, B., 2019. Understanding the interfacial interac-
- tions of bioinspired chitosan-calcite nanocomposites by first principles molecular dynam-
- ics simulations and experimental FT-IR spectroscopy. Carbohydrate Polymers 223, 115054.
- 726 https://doi.org/10.1016/j.carbpol.2019.115054
- 727 Zhuang, D., Yan, H., Tucker, M.E., Zhao, H., Han, Z., Zhao, Y., Sun, B., Li, D., Pan, J., Zhao, Y.,
- Meng, R., Shan, G., Zhang, X., Tang, R., 2018. Calcite precipitation induced by bacillus cereus
- MRR2 cultured at different Ca2+ concentrations: Further insights into biotic and abiotic cal-
- cite. Chemical Geology 500, 64–87. https://doi.org/10.1016/j.chemgeo.2018.09.018
- Zou, H., Pan, G., Chen, H., Yuan, X., 2006. Removal of cyanobacterial blooms in taihu
- lake using local soils II. Effective removal of microcystis aeruginosa using local soils
- and sediments modified by chitosan. Environmental Pollution 141, 201–205. https:
- //doi.org/10.1016/j.envpol.2005.08.042
- Zou, Z., Habraken, W.J.E.M., Matveeva, G., Jensen, A.C.S., Bertinetti, L., Hood, M.A., Sun, C.,
- Gilbert, P.U.P.A., Polishchuk, I., Pokroy, B., Mahamid, J., Politi, Y., Weiner, S., Werner, P.,
- Bette, S., Dinnebier, R., Kolb, U., Zolotoyabko, E., Fratzl, P., 2019. A hydrated crystalline
- calcium carbonate phase: Calcium carbonate hemihydrate. Science 363, 396–400. https:

739 //doi.org/10.1126/science.aav0210